X-ray photon storage in a crystal cavity

K.-D. Liss[a], R. Hock[b], M. Gomm[b], B. Waibel[c], A. Magerl[b], M. Krisch[a], R. Tucoulou[a]

[a]European Synchrotron Radiation Facility, B.P. 220, F-38043 Grenoble Cédex
[b]Lehrstuhl für Kristallographie und Strukturphysik, Universität Erlangen Nürnberg, D-91054 Erlangen
[c]MTU Motoren- und Turbinen-Union GmbH, D–80991 München

ABSTRACT

With the upcome of shorter and shorter time scales, time dependence of multiple diffraction effects will play a fundamental role in X-ray optics. Here we report on experimental X-ray photon storage in backscattering geometry between two silicon crystal slices cut from a monolithic ingot. The slices are 150 mm apart and wedge shaped to vary the diffracting thickness between 50 µm and 500 µm. A photon energy of 15.816 keV fulfills the condition for the 888 Bragg reflection. We used the dedicated backscattering beamline ID28 at ESRF which delivers a highly monochromatic beam equal to the natural width of the reflection considered. In Bragg condition, each crystalline boundary of the cavity has a probability of photon transmission and reflection, the ratio depending on the crystal thickness. Once a photon is transmitted by the first slice, it can be reflected by the second crystal and so on. A fast avalanche detector positioned behind the cavity detects the photons as a function of time with respect to the synchrotron bunches. Thus, photons that exit in direct transmission, or after N multiple forth and back bounces are separated by N times one nanosecond. Up to 14 reflections could be observed. The experiment demonstrates not only feasibility of photon storage in a crystal cavity which may be relevant in the X-ray optics for a free electron laser but it also points towards the importance of the time domain, where pulses shorter than the diffracting volume may be deformed and shaped considerably due to multiple scattering.

Keywords: monolithic crystal; perfect silicon; sub-nanosecond time resolution; backscattering; synchrotron bunches; X-ray delay line; Fabry-Perot interferometer; free electron laser;

1. INTRODUCTION

Nowadays, synchrotrons deliver X-ray flashes in the 50 ps – 100 ps range [1] while shorter pulses in the 50-100 fs range can be obtained by laser plasma X-ray sources [2-4]. The upcoming free electron laser operating in the self amplified spontaneous emission regime will deliver 100 fs flashes with a brightness and lateral coherence as never seen before [5-7] and technical developments are under consideration to select single modes of 1 fs duration by seeding a photon field into the laser undulator [8]. To take advantage of these source properties X-ray bunches will have to be shaped and engineered in time, to allow sophisticated pump-probe experiments like investigation of the dynamics in phase transitions [9-11] or the direct observation of coherent phonons [3, 12, 13] in physics, the breaking and formation of bonds in chemistry [14], the characterization of fundamental processes and atomic motions in molecular biology [15] or the investigation of the propagation of cracks in materials science [16].

In these new time scales, multiple diffraction processes will play an increasingly important role in the deformation of an X-ray bunch. When the extension of the scattering medium becomes comparable to the size of the length of the bunch, then photons being multiply forth and back diffracted will develop coherence effects and even the difference of phase and group velocities of the optical wave inside the medium start to play a role in the X-ray regime [17-19].

Besides reflectometry at grazing incidence, hard X-ray optics is mostly based on Bragg diffraction and the essential devices have been described several decades ago [20]. Modern instrumentation on synchrotron sources take use from it in finesse and sophisticated devices employing multiple diffraction, like the nested channel cut monochromator for extreme energy resolution in nuclear resonance spectroscopy is only one example [21]. However, time dependencies of the devices are rarely studied [22] and together with a closed loop beam path in a cavity as presented here they are a new fundamental and important issue [23-25].

correspondence: Email: liss@esrf.fr — WWW: http://www.esrf.fr/exp_facilities/ID15A/liss.html
further information: http://www.esrf.fr/exp_facilities/ID15A/science/resonator/

X-Ray FEL Optics and Instrumentation, Dennis M. Mills, Horst Schulte-Schrepping, John R. Arthur, Editors,
Proceedings of SPIE Vol. 4143 (2001) © 2001 SPIE · 0277-786X/01/$15.00

Crystal cavities and resonators may be carved out from a single crystal ingot as described in the beginning of the seventies of the last century [20, 26]. The geometry not only fixes the relationship between diffraction angle and photon energy as in Bragg's law but also the condition of the beam path. Like in visible optics, several modes may fit into a cavity and one has to distinguish between completely incoherent or coherent superposition of multiple diffracted parts of the wave, the latter leading to an interferometer. In the present study we consider the incoherent case of the simplest of such a cavity, namely two Bragg mirrors in exact backscattering geometry, such that a photon can be trapped and bounce forth and back several times [24].

2. TIME RESOLUTION

The salient feature of the present work is the time resolved study of the intensity leaving a crystal cavity exposed to a short X-ray flash. The stroboscopic acquisition principle presented two years ago [27] repeatedly measures the time delay between a registered photon and the bunch clock which triggers the delivery of the photon flash from the synchrotron.

In the time resolving synchrotron modes at ESRF N=32, 16 or 1 bunches are distributed uniformly in the storage ring. Out of 992 bunch positions only every 992/N-th position is filled while all others are suppressed by 10^{-6} or better. A bunch packet at a 5 mA filling lasts typically 100 ps and the arrival time is known very accurately relative to the bunch clock. In the present case the 16-bunch mode was used.

The detector consists of a fast silicon avalanche diode of about 10 µm thickness and 1 mm diameter. It's time resolution depends on the photon energy and is better than 1 ns. The device has been developed and characterized for nuclear resonance spectroscopy experiments and it has been described by Kishimoto [28].

The detector signal starts a clock, the time-to-amplitude converter which is then stopped by the trigger signal of the bunch clock, i. e. the remaining time from the photon event to the next photon delivery, but a phase is measured. This inverse mode is chosen since detector events occur much less frequently than trigger events of the 5.68 MHz bunch clock in 16 bunch mode. This method corresponds to a negative time axis of the multi channel analyzer. Stroboscopic repetition is accumulated until statistics are satisfied. The schematic flux diagram is presented in figure (1).

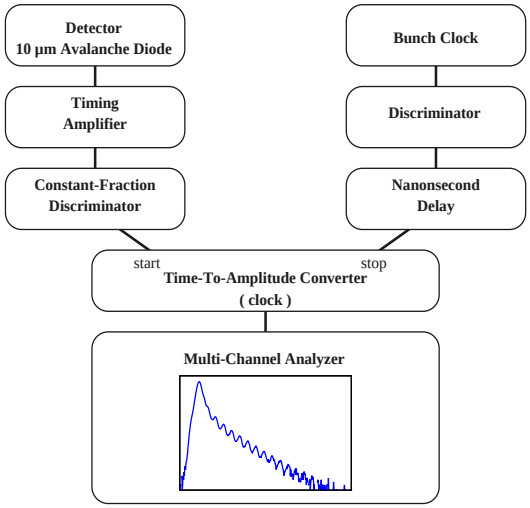

Figure (1): Block diagram of the timing electronics. The data acquisition is taken stroboscopically. The detection time of the photon is compared to the bunch clock of the synchrotron which gives the arrival time of the 100 ps X-ray flash. Same time delayed events are stored in the same channel of a multi channel analyzer while the procedure is repeated until sufficient statistics is obtained.

3. EXPERIMENTAL SETUP

The aim of the experiment was a study of X-ray photons stored between two thin, parallel crystalline plates in backscattering Bragg geometry. The inelastic scattering beamline ID28 at ESRF was chosen as it employs already a backscattering geometry for a very high resolution monochromator. A schematic overview is given in figure (2). The

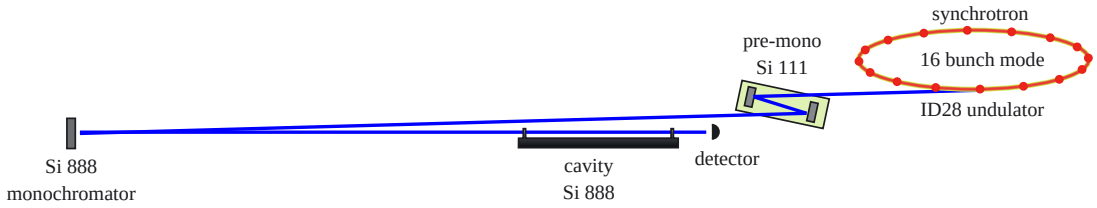

Figure (2) Scheme of the experimental setup for the X-ray photon storage experiment at the backscattering beamline ID28. X-ray flashes of 100 ps duration from the 16 bunch storage ring mode are monochromized with a Si 888 reflection in nearly backscattering geometry and impinge onto the cavity, which fulfills the Si 888 backscattering condition exactly. An avalanche diode detector is placed behind the device to measure the time structure of the transmitted beam.

Figure (3): Sketch of the cavity with the two active slices sticking out of the monolithic device within a distance of 150 mm. Photons impinging from the left can be trapped due to transmission and reflection probabilities T and R, respectively. They exit the cavity with probabilities TT, TRRT, TRRRRT ... T^2R^{2N} for 0, 1, 2 ... N back and forth bounces, being delayed by N times the time of flight inside the cavity of 1.0 ns. The reflection angle is adjusted to exactly 180 degree and the beam paths of multiply reflected photons are truly superimposed in space.

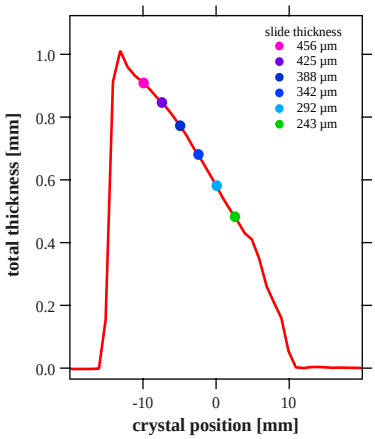

Figure (4): The crystal thickness along the wedge shaped slices has been calibrated by X-ray absorption off the Bragg reflection resulting in the diagram which shows the transmission through both plates. The large dots mark the thicknesses where time resolved patterns have been taken.

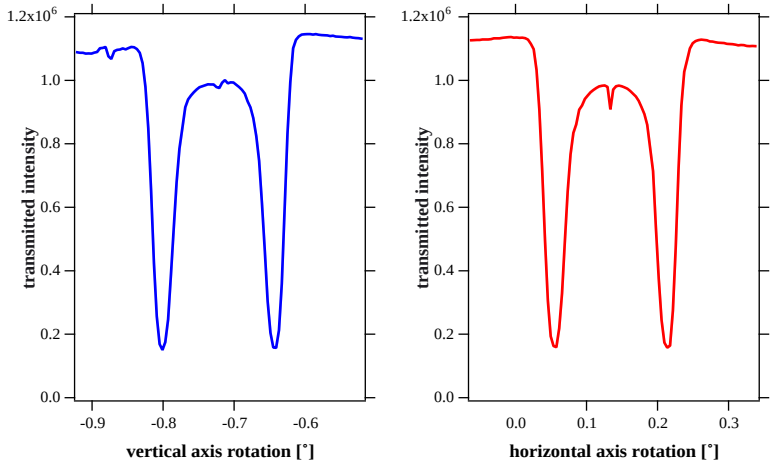

Figure (5): Alignment of the cavity takes place by detuning the monochromator to slightly higher photon energies than the silicon 888 Bragg condition in backscattering geometry. Thus the scattering angle is smaller than 180 degree and a rocking curve, taken by observation of the forward diffracted beam in transmission, shows two Bragg reflections, symmetrically around the 180 degree position. After the crystal is aligned, an energy scan with the monochromator can be taken. Note the small wiggles and dips as in the center between the large 888 dips stemming from other reflections which can be simultaneously excited being in exact 888 backscattering.

radiation from the undulator source passing a silicon 111 pre-monochromator was monochromatized using the silicon 888 reflection at a Bragg angle of 89.865°. This provided an X-ray beam of approximately 15.817 keV with an energy resolution of 3.7 meV and a divergence of about 10 µrad. The energy of the incoming photons could be varied through thermal expansion of the lattice spacing by an accurate temperature control of the monochromator, and an overall stability of typically 10 mK during the integration time of one pattern could be achieved. With the thermal expansion coefficient $\alpha = 2.56 \cdot 10^{-6}\ K^{-1}$ for silicon the relative lattice parameter uncertainty results in $\Delta d/d = \alpha\ \Delta T = 2.56 \cdot 10^{-8}$, a value much smaller than both the energy resolution $\Delta E/E = 2.3 \cdot 10^{-7}$ of the incident X-ray beam and the natural line width of the reflection.

The X-ray cavity consists of a pair of vertical plates cut from a monolithic silicon crystal, separated by 150 mm. The 111 orientation is along their surface normals, as sketched in figure (3). The plates are slightly wedge shaped in order to vary the

effective crystal thickness between approximately 50 µm and 500 µm by a horizontal translation perpendicular to the axis of the beam. The actual working thickness has been obtained by X-ray absorption measurements on the diffractometer off the Bragg reflection as presented in figure (4).

The cavity was aligned such that the beam is reflected exactly back into the axis of the incident beam. This has been achieved by detuning the incident photon energy to slightly higher values, such that the Bragg angle is less than 90°. The prealigned crystal is then rocked successively around the two axes perpendicular to the beam. This yields two local minima of the intensity as shown in figure (5) corresponding to the Bragg conditions where intensity is scattered off the transmitted beam. The mid positions of these Bragg peaks are the orientations where the lattice planes are aligned perpendicular to the incident beam.

The Bragg condition for the cavity was determined by energy variation of the incoming photons via the controlled thermal expansion of the monochromator lattice spacing. A scan is shown in figure (6). The exact Bragg condition is fulfilled when the transmitted intensity has a minimum, since most of the photons are then back reflected and do not reach the detector. The observed Full-Width-Half-Maximum (FWHM) on the relative energy scale is $\Delta E/E = 7.4 \cdot 10^{-7}$ and the minimum transmission through the two 292 µm slices is 17 % after consideration of normal absorption. The theoretical widths for the reflection and transmission curves can be calculated by standard dynamical theory of diffraction without absorption where the deviation from the Bragg condition has to be expressed as a longitudinal variation of the scattering vector [29] which then is valid also in exact backscattering geometry. To model the exact shape including the asymmetry near the Bragg condition, however, needs to take into consideration absorption. Although standard programs like XOP exist [30], they have the disadvantage not to work in exact backscattering geometry. The asymmetry, i. e. the different height of the background to the right and the left of the dip are well reflected in the experimental data and are proof for the quality of the crystal. Moreover we note that the FWHM is slightly larger than the theoretical values for the convolution of the transmission curve with the reflection curve of the monochromator.

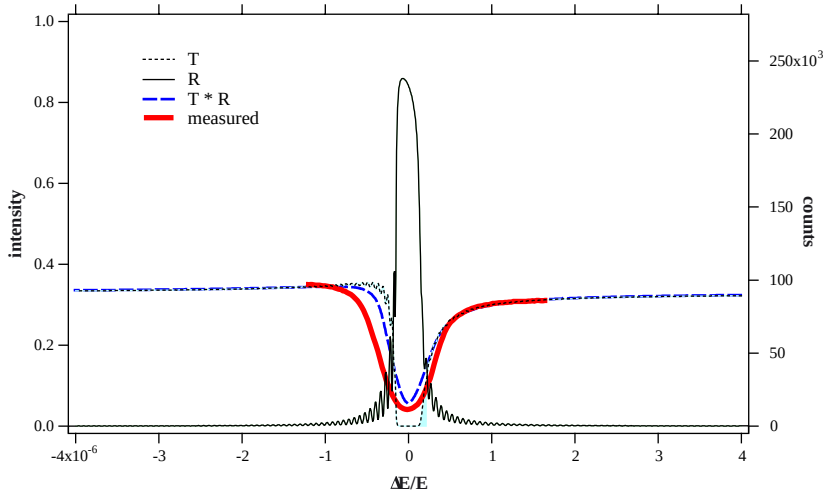

Figure (6): Calculated reflection and transmission curves R and T of a 2 x 292 µm thick crystal as a function of energy deviation from the center of the Bragg reflection are shown by the thin continuous and dotted lines, respectively. The monochromator delivers a similar curve to R, regardless of the small wiggles stemming from the slice thickness, thus the calculated curve for the simulation of an energy scan is the convolution T*R, the thick, dashed line. The experimental data represented by the thick, continuous line have been adapted to the intensity scale only. The asymptotic to the blue curve is the absorption far off the Bragg peak while experimental data is consistent with theory for anomalous absorption, the asymmetry around the Bragg position.

4. RESULTS

The time dependence of the transmitted beam at the center of the Bragg reflection, i. e. at the dip in figure (6), is shown in figure (7) for various crystal thicknesses. Figure (7a) shows the time structure of the detector without the cavity in the beam. The intensity maximum corresponds to the undelayed photons at t = 0. The signal has a FWHM of 500 ps corresponding to the time response of the detector. The shape asymmetry arises from intrinsic capacities. This does not bear any relevance for the present experiment and it will not be discussed further [28]. The time patterns with the cavity in the Bragg position differ qualitatively from the first curve and show a series of sequential maxima separated by 1.0 ns forming

an exponential decay towards longer times. The maxima correspond to photons trapped within the cavity for 1, 2, 3 ... N successive reflections from both crystal plates. When the beam impinges onto the first crystal slice, there is a probability for transmission, giving the forward diffracted beam. The same holds for the second plate and therefore yields a maximum signal at t = 0. But there is also a probability for reflection at each slice, permitting part of the beam to go back and forth and thus to travel several times the distance between the slices, i. e. multiples of 30 cm or of 1.0 ns in time, corresponding to the detected peak separations. We observe clearly up to 14 peaks i. e. up to 14.0 ns of time delay.

The intensities strongly depend on the thickness of the crystal slices and time integrated intensities are plotted in figure (8). They follow well the exponential law with a decay coefficient of $\mu_{obs} = 47.25\ cm^{-1}$ situated well between the limits of pure absorption with $\mu_{abs} = 20.41\ cm^{-1}$ and the dynamical extinction with $\mu_{dyn} = 281\ cm^{-1}$ exactly at the Bragg position.
The intensity ratios of successive back and forth bounces are given in figure (9).They demonstrate, that most of the intensity leaks off the cavity within the first few bounces, while a high asymptotic value of 0.5 is obtained for higher reflections.

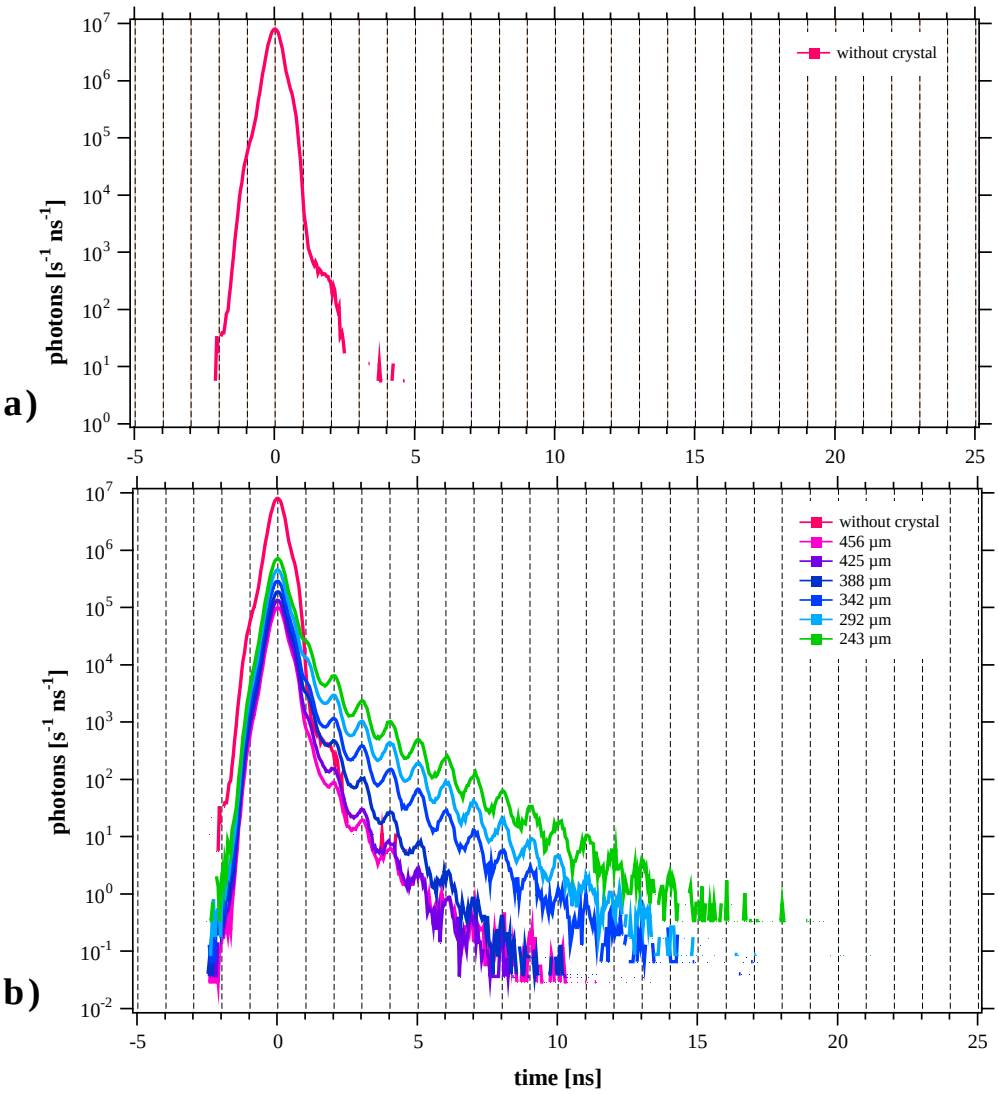

Figure (7): Time patterns of stored photons at the exit of the cavity. Without the crystal in the beam, only a direct bunch of photons is observed at time 0 (a) with a width of 500 ps corresponding to the time resolution of the avalanche detector. Many delayed bunches appear when the device is in Bragg condition (b). Each peak in later times correspond to multiple back and forth travels inside the device while the stored intensity depends on the crystal thickness.

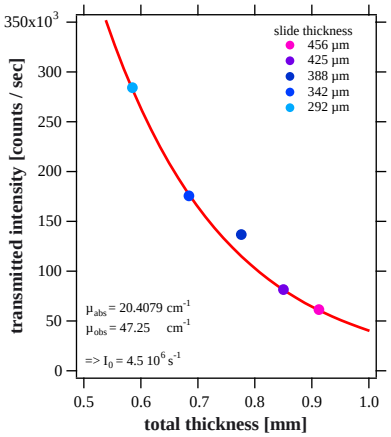

Figure (8): The view graph shows the integrated intensities of the time patterns of figure (7). Since they have been measured in Bragg condition, they show higher extinction μ_{obs} than in the absorption case μ_{abs}. The exponential extrapolation to zero thickness gives the value for the incident photon intensity to the cavity.

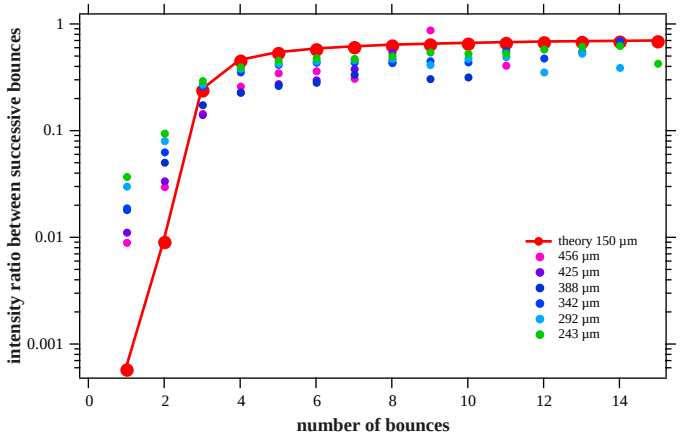

Figure (9): Intensity ratios between neighboring peaks in time of figure (7) and calculated values obtained from dynamical theory.

5. SIMULATION

The bounce ratios regarding the reflection and transmission curves have been simulated by a simple model within the framework of dynamical theory neglecting absorption,

$$R_B(y, A) = \frac{1}{y^2 + (y^2 - 1)\cot^2\left(A\sqrt{y^2 - 1}\right)} \quad \text{and} \quad T_B(y, A) = 1 - R_B(y, A)\ , \tag{1}$$

respectively. Here y is the deviation from the Bragg condition in both angular (transverse) and energy (longitudinal) space [29] and $A = \pi\ D / \Delta_0$ the dimensionless unit for the crystal thickness D where $\Delta y = 1$ is the half width of the Darwin plateau and $A = \pi$ corresponds to one Pendellösung period Δ_0 [29, 31-33]. Successively transmitted and reflected intensities are calculated by pointwise multiplication. For the N-th bounce e. g., two transmissions to enter and exit the cavity with 2N reflections in-between are considered, i. e.

$$T_N(y, A) = T_B^2(y, A)\, R_B^{2N}(y, A)\ . \tag{2}$$

Figure (10) displays the results for a thickness $A = \pi$ for each slice. The reflectivity almost reaches 100% in the center while the transmission curve has a minimum of 0.8% which propagates through the higher order bounces. This demonstrates the difficulty of entering and leaving the cavity. Most of the intensity is stored at the border/edges of the Darwin plateau, where reflectivity is starting to decrease while transmission increases. The integrated reflectivities lead to the

curves given in figure (11) as a function of crystal thickness. These intensities peak between 0.5 and 1.5 Pendellösung thicknesses depending on the order of bounces. For a small number of reflections one can accept a smaller reflectivity in advantage of transmission to enter and exist the cavity. High orders, however, need high reflectivity since it enters potentially into the formula (2).

The ratios of the integrated values from the curves in figure (10) lead to the theoretical bounce ratios compiled with the experimental data in figure (9).

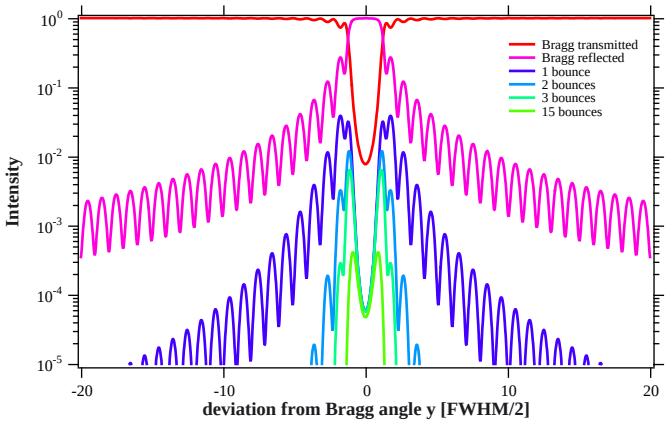

Figure (10): Theoretical transmission and multiple reflection curves for 2 x 150 µm thick crystals as a function of the deviation from the Bragg position as obtained from simple dynamical theory of diffraction without absorption.

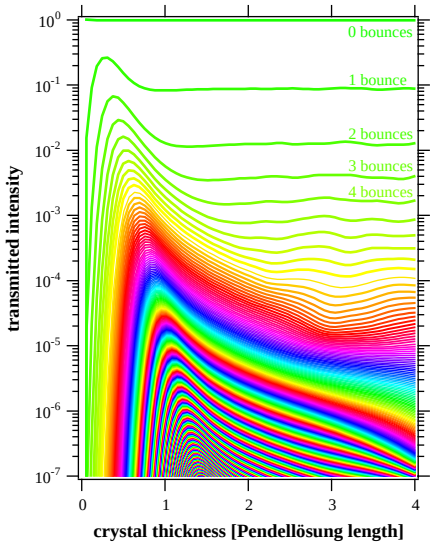

Figure (11): Intensity calculations by integration of the curves in figure (10) for multiple reflected photons as a two- dimensional function of crystal thickness and number of bounces. Although reflectivity is high for thick crystals, transmission and thus the probability to enter and leave the cavity is low, while transmission becomes good and reflectivity unfavorable for thinner crystals. The optimal crystal thickness depends on the number of bounces and is about one Pendellösung period when long photon storage times are desired. For a very few number of bounces the optimum thickness moves to thinner crystals, about half a Pendellösung period in favor for higher transmission and reduced reflectivity.

6. DISCUSSION

The experimental data fit well the simulation. In particular the higher order bounce ratios reach the same order of magnitude. The simulated values are still about 20% higher certainly due to the neglected photo absorption. For the first few bounces the experimental values are considerable higher than simulated. We interpret this by the existence of strain fields in the

Czochralski grown crystal allowing some broader intensity profile around the Bragg line as confirmed by the wider transmission curve in the energy scan of figure (6).

Much of the primary intensity is lost due to the low transmission in the center of the reflection curve, where photons cannot enter or leave the cavity. Thus most of the intensity is stored in the wings of the Bragg profile.

Similar devices have been developed for neutron storage [34] using the Zeemann effect for a magnetic energy shift while the radiation enters the cavity [35]. X-rays, however, do not have this advantage and time scales for a switch have to be five orders of magnitude faster. Possible onsets to overcome the transmission gating problem is to shift the crystal reflection properties by an acoustic wave which may be induced by a well triggered laser pulse.

The simulations have been simplified to the so called two-beam case in dynamical theory of diffraction while the silicon 888 reflection in exact backscattering geometry is characterized by an eight-beam case. This might raise the discussion whether photon storage in this geometry is feasible at all. Although this problem has been studied on several reflections [36] the Si 888 case has so far not been treated in theory. Qualitative interpretation obtained from other reflections [37] reveal that the multiple beam case is restricted to a narrow region effecting only the center of reflectivity region of the two-beam case in both transverse and longitudinal space. Thus, even at exact backscattering storage should be well possible.

7. APPLICATIONS

The reported experiment is fundamental for applications employing all kinds of photon storage at X-ray energies as well as for the time dimension in diffraction processes. Even if a diffraction process can be studied in detail in a time averaged way it will reveal additional and novel information by using the additional dimension of time [27].

For example, a Fabry-Perot interferometer as proposed by several groups [38, 39] is a device to narrow a transmission line by interference of multiply diffracted parts of the same wave field. In this case wave trains much longer than the length of the crystal cavity and a spacing of the slices about a Pendellösung period is needed. The reflection process, however, is the same as in the present device and can be studied in detail with the present incoherent multiple reflection geometry. The time resolution serves as a unique means to separate multiple reflected packets. A Fabry-Perot interferometer with a coherent superposition of the wave fields in the cavity length scales some one thousand times smaller and a time resolution some one thousand times better will be necessary for temporal investigation. There is promise to reach these new dimensions within the coming decades with the developments of free electron lasers. Then interplay of monochromatization and temporal deformation of light pulses will play a tremendously important role.

Free electron lasers will need different kinds of delay lines and storage devices. A typical time pattern as proposed for the X-FEL at DESY is shown in figure (12). The separation of succeeding photon bunches will be some 100 ns while experiments may need shorter repetition like in shock wave physics [11] where the sample is destroyed through the pumping

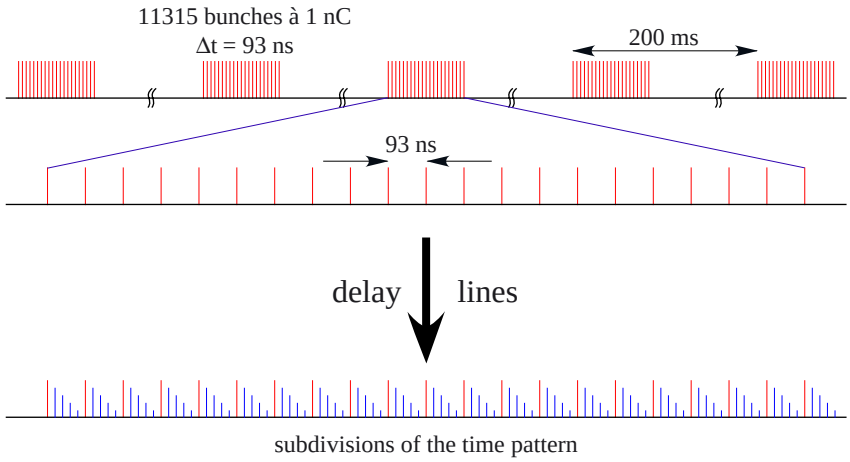

Figure (12): Proposed time pattern for the German X-FEL project which delivers 100 fs X-ray pulses with a repetition rate of 93 ns. A series of experiments would need higher repetition rates adapted to the physical process to be studied, a gap which could be overcome with photon storage devices [7].

mechanism within this time. This can be achieved on the basis of the presented storage device by adapting the length to the desired time separation. Furthermore such optics is not restricted to closed loop devices. This may overcome the entrance problem and crystals with multiple exit holes selecting different delayed beam paths across its section as in figure (13) can be envisaged. However the different delayed parts exit the device at different locations such that a need to redirect the beam may arise.

An application along similar lines can be considered for a seeding procedure of a free electron laser. The principle is given in figure (14) with the amplifying device, the FEL undulator. Usually electrons arriving from the left start with spontaneous emission in the first part while this radiation is amplified by stimulated emission in the last section of the undulator. Seeding is the process to bring into the undulator a well defined photon wave field which then becomes amplified. The properties of this seeding wavefield then determines the wavefield at the exit with respect to coherence, frequency and time pattern [8]. One possibility for seeding is to employ a second undulator which then delivers photons to be optically shaped for the seeding of the FEL undulator, while another possibility would be to take off some of the intensity of the FEL exit beam by a crystal mirror, send it back to the entrance and seed a later electron bunch. Such a device, resembles to the crystal cavity, maybe with a hole at the exit to avoid damage by the intense X-ray beam feeding back only a coronal part of the beam. Detailed calculations have to be done for the geometry which is not necessarily restricted for the backscattering case, for the phase space matching, for the power densities or for the influence of the optics to the coherency quality of the X-ray beam delivered.

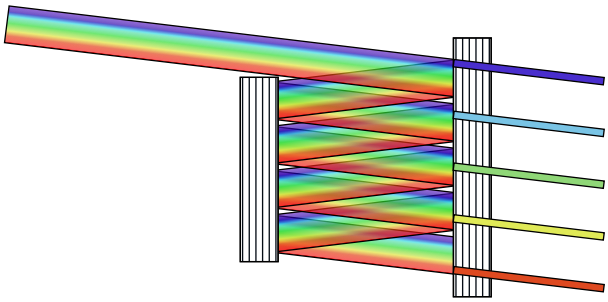

Figure (13): Open loop delay line. Photons are reflected back and forth between two parallel crystals and are delayed by this process. Holes in one of the crystals select different parts of the cross section of the original beam with different delays.

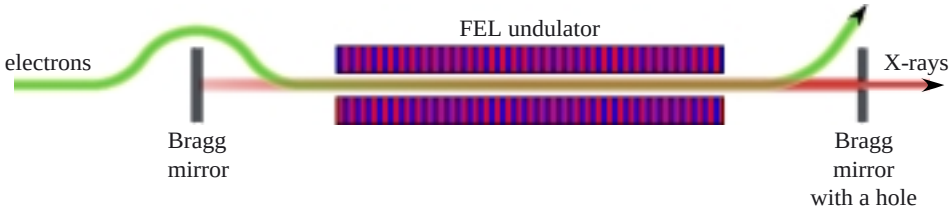

Figure (14): Scheme of a FEL feedback system for seeding. Part of the X-ray beam at the exit of the FEL undulator is reflected back to its input which seeds the photon wave field to be amplified for a synchronized incoming electron bunch.

8. CONCLUSION

In this very fundamental experiment we have demonstrated the storage of photons up to 14 ns with so far highest energies. High intensity ratios of up to 50 % between neighboring bounces have been observed. Higher number of bounces were observed with thinner crystals. Discrepancies between the observed time patterns of transmitted intensity and calculations based on the dynamical theory of diffraction are most likely due to a slightly distorted cavity crystal. Based on this concept devices like the Fabry-Perot interferometer or storage and delay lines for the free electron laser optics can be developed. Future investigations should focus on the optimized conditions for photon storage and the problem to enter and leave the cavity. Applications are not necessary limited to backscattering geometry as proposed generally for X-ray resonators with a closed loop ray path [26].

ACKNOWLEDGMENTS

The crystal device has been manufactured by the optics group of ESRF manly by the sure hands of André Paul to whom we deeply wish to express our thanks.

REFERENCES

1. J.-L. Revol, E. Plouviez, R. Rüffer, "The ESRF timing system and single bunch operation" Synchrotron Radiation News, **7**(4): p. 23-28, 1994.
2. A. Rousse, C. Rischel, I. Uschmann, P. A. Albouy, J.-P. Geindre, P. Audebert, J.-C. J. Gauthier, E. Förster, J.-L. Martin, A. Antonetti, "Femtosecond time-resolved X-ray diffraction with a laser-produced plasma x-ray source" Proceedings of SPIE, **3451**: p. 22-29, 1998.
3. J. Wark, "Table-top picosecond sources" Nature, **398**: p. 284-285, 1999.
4. C. Reich, P. Gibbon, I. Uschmann, E. Förster, "Yield optimization and time structure of femtosecond laser plasma Kα sources" Physical Review Letters, **84**(21): p. 4846-4849, 2000.
5. J. Rossbach, "A VUV free electron laser at the TESLA test facility at DESY" Nuclear Instruments and Methods in Physics Research, **A**(375): p. 269-273, 1996.
6. M. Cornaccia, "LCLS X-ray FEL at SLAC" SPIE Proceedings, **3614**: p. 109-118, 1999.
7. T. Tschentscher, W. Drube, H. Franz, R. Gehrke, H. Schulte-Schrepping, T. Wroblewski, G. Materlik, "Parameters and example applications for the X-FEL at DESY". Report, , HASYLAB at DESY, 2000. http://www-hasylab.desy.de/workshops/additional_mat.htm
8. E. L. Saldin, E. A. Schneidmiller, M. V. Yurkov, "Optimization of a seeding option for the VUV free electron laser at DESY" Nuclear Instruments and Methods in Physics Research, **A**(445): p. 178-182, 2000.
9. J. S. Wark, "Time-resolved X-ray diffraction" Contemporary Physics, **37**(3): p. 205-218, 1996.
10. J. Larsson, P. A. Heimann, A. M. Lindenberg, P. J. Schuck, P. H. Bucksbaum, R. W. Lee, H. A. Padmore, J. S. Wark, R. W. Falcone, "Ultrafast structural changes measured by time-resolved X-ray diffraction" Applied Physics, **A**(66): p. 587-591, 1998.
11. T. d'Almeida, Y. M. Gupta, "Real-time X-ray diffraction measurements of the phase transition in KCl shocked along [100]" Physical Review Letters, **85**(2): p. 330-333, 2000.
12. C. Rose-Petruck, R. Jimenez, T. Guo, A. Cavalleri, C. W. Siders, F. Ráksi, J. A. Squier, B. C. Walker, K. R. Wilson, C. P. J. Barty, "Picosecond-milliångström lattice dynamics measured by ultrafast X-ray diffraction" Nature, **398**: p. 310-312, 1999.
13. A. M. Lindenberg, I. Kang, S. L. Johnson, T. Missalla, P. A. Heimann, Z. Chang, J. Larsson, P. H. Bucksbaum, H. C. Kapteyn, H. A. Padmore, R. W. Lee, J. S. Wark, R. W. Falcone, "Time-resolved X-ray diffraction from coherent phonons during a laser-induced phase transition" Physical Review Letters, **84**(1): p. 111-114, 2000.
14. F. Ráksi, K. R. Wilson, Z. Jiang, A. Ikhlef, C. Y. Côté, J.-C. Kieffer, "Ultrafast X-ray absorption probing of a chemical reaction" Journal of Chemical Physics, **104**(15): p. 6066-6069, 1996.
15. B. Perman, V. Srajer, Z. Ren, T.-Y. Teng, C. Pradervand, T. Ursby, F. Schotte, M. Wulff, R. Kort, K. Hellingwerf, K. Moffat, "Energy Transduction on the Nanosecond Time Scale: Early Structural Events in a Xanthopsin Photocycle" Science, **279**: p. 1946-1950, 1998.
16. C. J. SHIH, M. A. MEYERS, V. F. NESTERENKO, S. J. CHEN, "Damage evolution in dynamic deformation of silicon carbide" Acta Materialia, **48**(9): p. 2399-2420, 2000.
17. R. Tatchyn, "Synchrotron radiation optics in the short pulse limit: design implications for the SLAC Linac Coherent Light Source (LCLS)" SPIE Proceedings, **3773**: p. 180-191, 1999.
18. J. Wark, "Femtosecond X-ray diffraction: experiments and limits" SPIE Proceedings, **4143**: p. in this issue, 2000.

19. J. S. Wark, R. W. Lee, “Simulations of femtosecond X-ray diffraction from unperturbed and rapidly heated single crystals” Journal of Applied Crystallography, **32**: p. 692-703, 1999.

20. M. Hart, “Bragg reflection X-ray optics” Reports on Progress in Physics, **34**: p. 435-490, 1971.

21. T. M. Mooney, T. Toellner, W. Sturhahn, E. E. Alp, S. D. Shastri, “High-resolution, large-angular-acceptance monochromator for hard X-rays” Nuclear Instruments and Methods in Physics Research, **A**(347): p. 348-351, 1994.

22. S. Joksch, W. Graeff, J. B. Hastings, D. P. Siddons, “Performance of an X-ray optical time delay line with synchrotron radiation” Review Scientific Instruments, **63**: p. 1114-1118, 1992.

23. R. Smith, “Making hard light sharper” Nature, **404**(6776): p. 345-347, 2000.

24. K.-D. Liss, R. Hock, M. Gomm, B. Waibel, A. Magerl, M. Krisch, R. Tucoulou, “Storage of X-ray photons in a crystal resonator” Nature, **404**(6776): p. 371-373, 2000.

25. B. Cernik, “Making the most of synchrotrons” Physics World, **13**(7): p. 26-27, 2000.

26. R. D. Deslattes, “X-ray monochromators and resonators from single crystals” Applied Physicd Letters, **12**(4): p. 133-135, 1968.

27. K.-D. Liss, A. Magerl, R. Hock, B. Waibel, A. Remhof, “The investigation of ultrasonic fields by time resolved X-ray diffraction” Proceedings of SPIE, **3451**: p. 117-127, 1998.

28. S. Kishimoto, “An avalanche photodiode detector for X-ray timing measurements” Nuclear Instruments and Methods in Physics Research, **A**(309): p. 603-605, 1991.

29. K.-D. Liß, “Strukturelle Charakterisierung und Optimierung der Beugungseigenschaften von $Si_{1-x}Ge_x$ Gradientenkristallen, die aus der Gasphase gezogen wurden”. Dissertationsschrift, Rheinisch Westfälische Technische Hochschule Aachen, 1994. http://www.esrf.fr/exp_facilities/ID15A/theses/DissLiss/Zusammenfassung.html

30. M. Sanchez del Rio, R. J. Dejus, “XOP - X-ray oriented programs”. http://www.esrf.fr/computing/scientific/xop/

31. W. H. Zachariasen, *“Theory of X-Ray diffraction in Crystals”* John Wiley and Sons: London. 1945.

32. H. Rauch, D. Petrascheck, “Grundlagen für ein Laue-Neutroneninterferometer Teil 1: Dynamische Beugung”. AIAU 74405b, Atominstitut der Österreichischen Universitäten, 1976.

33. H. Rauch, D. Petrascheck, “Dynamical neutron diffraction and its application” in *“Neutron Diffraction”*, H. Dachs, Editor. Springer-Verlag: Berlin Heidelberg New York. p. 303-351, 1978.

34. M. R. Jäkel, C. J. Carlile, E. Jericha, D. E. Schwab, H. Rauch, “New Measurements with a Perfect Crystal Cavity for Neutrons” Proceedings of SPIE, **3767**: p. 353-359, 1999.

35. M. Schuster, H. Rauch, E. Seidl, E. Jericha, C. J. Carlile, “Test of a perfect crystal neutron storage device” Physics Letters, **A**(144): p. 297-300, 1990.

36. J. P. Sutter, “Applications of special X-ray diffraction cases in silicon crystals”. doctoral thesis, Purdue University, 2000.

37. V. G. Kohn, I. V. Kohn, É. A. Manykin, “Diffraction of X-rays at a Bragg angle of $\pi/2$ (back reflection) with consideration of multiwave effects” Journal of Experimental and Theoretical Physics, **89**(3): p. 500-507, 1999.

38. A. Steyerl, K.-A. Steinhauser, “Proposal of a Fabry-Perot-type interferometer for X-rays” Zeitschrift für Physik, **B**(34): p. 221-227, 1979.

39. A. Caticha, S. Caticha-Ellis, “A Fabry-Perot interferometer for hard X-rays” Physica Status Solidi, **A**(119): p. 643-654, 1990.